Available online at www.sciencedirect.com
ScienceDirect
Trans. Nonferrous Met. Soc. China 33(2023) 2136−2154
Transactions of Nonferrous Metals Society of China
www.tnmsc.cn

Bionanocomposites containing SnO_2 with improved chemical resistance and hydrophobic behaviours for applications in food packaging industry

Joseph Raj XAVIER[1], C. DHANALAKSHMI[2], Shanmuga Sundari CHANDRARAJ[2], S. P. VINODHINI[1]

1. Department of Chemistry, Saveetha School of Engineering,
Saveetha Institute of Medical and Technical Sciences, Chennai-602 105, Tamil Nadu, India;
2. Department of Chemistry, Vel Tech Rangarajan Dr. Sagunthala R&D Institute of Science and Technology,
Chennai-600 062, Tamil Nadu, India

Received 1 March 2022; accepted 8 June 2022

Abstract: The influence of poly(asparagine-co-phenylalanine) (P(Asn-co-Phe)/SnO_2) on the protection performance of epoxy coating was investigated. The electrochemical impedance spectroscopy (EIS) analysis indicates the better protection against coating degradation of epoxy (EP)−P(Asn-co-Phe)/SnO_2 nanocomposite on tinplate compared to that of pure epoxy coatings. The coating resistance (R_{coat}) of the EP−P(Asn-co-Phe)/SnO_2 nanocomposite is found to be 3854.70 kΩ·cm^2. The R_{coat} of EP−P(Asn-co-Phe)/SnO_2 nanocomposite coating is found to be over 38 times greater than that of the EP coating. Scanning electrochemical microscopy (SECM) analysis shows less current distribution for the EP−P(Asn-co-Phe)/SnO_2. The analyses of degradation products by XRD and SEM/EDX confirm the influence of functionalized SnO_2 particles on the protecting ability of epoxy coating. The hydrophobic nature of the EP−P(Asn-co-Phe)/SnO_2 nanocomposite coating (θ=133°) is confirmed by water contact angle measurement. The resultant nanocomposite coatings display enhanced mechanical properties. The results show that the EP−P(Asn-co-Phe)/SnO_2 nanocomposite in wells increased the antibacterial activity as compared with pure EP. Therefore, it is concluded that the newly synthesized EP−P(Asn-co-Phe)/SnO_2 nanocomposite provides an outstanding barrier and mechanical properties due to the addition of P(Asn-co-Phe)/SnO_2 nanoparticles to the epoxy matrix, which obstructs the degradation of materials and assists in prolonging the life of the coated steel.

Key words: tinplate; epoxy; SnO_2; nanocomposite coatings; copolymer; thermal stability; hardness

1 Introduction

The food packaging protects food from the environmental contamination and other influences such as odours, shocks, dust, temperature, physical damage, light, microorganisms, and humidity, and it is essential for ensuring food quality and safety, as well as extending shelf-life and reducing food losses and waste [1]. Tinplate is the most common coated steel used in food packaging [2] for food preservation and long-term safe food storage [3]. Tinplate is steel (base steel) that has been coated with tin on both sides. Tinplate is less expensive and heavier than aluminium, but it is also recyclable and simple to decorate. It possesses a magnetic characteristic that aids in separation and is water and gas resistant. It can also withstand high temperatures during product processing, making it appropriate for long-term storage of sterile products like beverages [4]. When exposed to hostile foods, tinplate possesses microstructural discontinuities such as surface porosity and defects, which are ideal corrosion sites [5]. It does, however, require surface coatings because it may react with food, and accessing the product from its containers usually

Corresponding author: Joseph Raj XAVIER, Tel: +91-94-4448-9845, E-mail: drjosephrajxavier@gmail.com
DOI: 10.1016/S1003-6326(23)66249-1

necessitates the use of an opener [6]. Because of its outstanding mechanical properties, excellent chemical resistance, thermal stability, and adhesive nature, thermoset resins are widely employed as coatings to protect metal substrates from corrosion, as well as primers for precoated steel sheets used in a variety of applications [7]. Because of their high degree of crosslinking, epoxy resins have been widely employed in coatings for food industry [8]. It is brittle, which means that epoxy composites have low impact strength and epoxy-based adhesives have low shear strength [9]. Because of its outstanding processability, strong adhesion, high mechanical strength, good thermal properties, excellent chemical resistance, good design flexibility, and ease of application, epoxy resin materials have been used as a matrix of anti-corrosive coatings of polymeric nanocomposites. Epoxy coatings are used as tin can linings in the food sector to avoid direct contact between food and metal surfaces, which causes chemical reactions [10].

It was found that combining two distinct polymers improves the physico-chemical and barrier properties for food applications. Researchers are very interested in bio-based and biodegradable polymers because they are environmentally benign and renewable. Due to their great transparency, chemical resistance, and gas barrier qualities, copolymers have been used in food packaging in several studies. The mechanical and antibacterial capabilities of pure chitosan film are insufficient for food packaging. Chitosan is combined with gelatin to improve its mechanical, thermal and barrier properties and utilised in food packaging. The fundamental disadvantage of ethylene vinyl alcohol copolymer is its moisture content sensitivity, which causes thermal, barrier, and mechanical properties to be reduced [11−13]. The poly(asparagine-co-phenylalanine) copolymer is used for this investigation due to the following two factors: (1) The biobased copolymer poly(asparagine-co-phenylalanine) P(Asn-co-Phe) exhibits several beneficial properties like aqueous solubility, chiral recognition, high biocompatibility, stimuli responsiveness, and antifouling properties; (2) Due to their unique amino-acid sequence and composition, these bio-inspired materials also possess unique properties such as the possibility to self-assemble via non-covalent interactions.

The addition of nanoparticles improved the thermomechanical performance of biopolymers, the wettability of the polymer surface, the property of hydrophobicity, the mechanical properties, the barrier properties, and the antimicrobial activity. Montmorillonite (MMT), zinc oxide (ZnO-NPs) covered silicate, kaolinite, silver NPs (Ag-NPs), and titanium dioxide (TiO_2−NPs) are the most common nanomaterials used in food packaging, as well as aluminium oxide and metalloid-based silicon dioxide [14−16]. Due to its wide surface area, tin oxide (SnO_2) has obtained essential features such as biocompatibility, chemical resistance, antioxidant, antibacterial [17], stability towards reducing gases [18], low cost, and good repeatability. The mechanical, barrier, and thermal degradation characteristics of poly(butylene adipate-co-terephthalate)/SnO_2 (PBAT/SnO_2) were all good [19]. Because of the interaction of Sn^{4+} with the amide and imide groups of polyanilines (PANI), PANI/chitosan/SnO_2 has a higher thermal stability [20]. Because of the presence of SnO_2 nanoparticles in the composite coatings, the epoxy (EP)/PANI/SnO_2 exhibits high corrosion resistance of A-36 steel due to the formation of a better oxygen permeability barrier, improved mechanical properties, improved adhesion, elastic modulus, tensile strength, and smart anti-corrosion formulations in protecting A-36 steel against harsh environments [21]. Metal oxide nanocomposites coated with PANI/epoxy/SnO_2 metal oxide nano-composites give substantial corrosion resistance [22]. In seawater, surface modified NiO−epoxy nano-composite showed good anticorrosive activity on mild steel [23]. Lysine (LY)−GO/EP had superior barrier qualities as well as better anti-corrosion properties [24]. For food packaging applications, poly (3-hydroxybutyrate-co-3-hydroxyvalerate)/ZnO showed better barrier performance, as well as good mechanical and thermal properties [25,26].

The goal of this project is to develop nanocomposites containing poly(asparagine-co-phenyl alanine) (P(Asn-co-Phe)) modified SnO_2 and epoxy resin for use in packaging films, and to determine the effect of epoxy resins and SnO_2 concentrations on the barrier, mechanical, and thermal properties of epoxidized films containing P(Asn-co-Phe) modified SnO_2 nanoparticles in the context of their potential use in food packaging. Thermal, mechanical, morphological, and chemical

resistance tests are used to investigate the effect of 4 wt.% SnO_2 on resin curing behaviour.

2 Experimental

2.1 Materials

The substrate is made of tinplate. Sigma–Aldrich provided the diglycidyl ether of bisphenol A (DGEBA) epoxy resin and the amine-containing hardener (Epikure F205). P(Asn-co-Phe) was used as a chemical modifier reagent. Ethanol and acetyl acetone (AcAc) were also used for the synthesis of nanocomposites. Merck Chemicals provided 98.0% acetone, which was utilised as received.

2.2 Preparation of nanocomposites

The sol–gel process was used to make the SnO_2 nanoparticles. 8 g hydrated tin chloride ($SnCl_2{\cdot}2H_2O$) was dissolved in pure ethanol in a usual process (C_2H_5OH). In a closed three-necked flask, the solution was agitated for 30 min using a magnetic stirrer. For the hydrolysis of SnO_2, around 5 mL of acetyl acetone (AcAc) was added drop by drop. The solution was refluxed at 800 °C for 5 h after 30 min to generate the SnO_2 sol solution. P(Asn-co-Phe) was used as a chemical modifier reagent, and 1 mL was added to the SnO_2 solution and aged at 300 °C for 72 h. The sol was dried at 1000 °C for 30 min before being calcined at 450 and 600 °C for 1 h to generate SnO_2 nanoparticles [27]. To obtain a stable system, the functionalized P(Asn-co-Phe)/SnO_2 nanoparticles were mixed separately with epoxy resin and aliphatic amine hardener (3:1) in a magnetic stirrer (3000 r/min) for 1 h. By adding various mass fractions of functionalized SnO_2 nanoparticles (1−5 wt.%) to the pure epoxy (EP) coating, several formulations of nanocomposite coatings were created. Tin plate was coated with EP, EP−SnO_2, EP−P(Asn-co-Phe), and EP−P(Asn-co-Phe)/SnO_2. The epoxy resin utilised in this study is classified as a fast-drying type epoxy in the industry. The liquid epoxy resin was made up of a combination of multifunctional low molecular mass diluents and bisphenol A's diglycidyl ether, while the curing agent was made up of aliphatic amines. The epoxy resin was used in a 3:1 mass ratio with the curing agent. The EP−based nanocomposite was coated on the tinplate specimen using spin coater. A coating without nanoparticles was also prepared for comparison. The coated specimen was kept at 50 °C for 5 d and stored in desiccators for at least three weeks before the analysis. The thickness of the coatings was found to be (40±2) μm as measured by Minitest 600 Erichen digital meter. The corrosion resistance and mechanical properties of the epoxy nanocomposites were tested. Uncoated and coated specimens were submerged in 0.1 mol/L HCl for 1, 24, 120, and 240 h, respectively [28].

2.3 Characterisation of modified SnO_2

The thermal properties of SnO_2 and P(Asn-co-Phe)/SnO_2 were evaluated by TGA (Model NETZSCH STA 449 F3 JUPITER). The crystalline size of the nanoparticles was determined using X-ray diffraction studies (XRD, PW−1840, Philips, Cu K, 40 kV, 30 mA). SEM/EDX procedure from ZIESS Germany was used to evaluate the product's surface shape and content. The FTIR spectroscopy was used to confirm SnO_2 and P(Asn-co-Phe)/SnO_2 composite produced. The AFM observation was carried out three times on separate samples using a 20 lm scanner in tapping mode to guarantee the authenticity of the findings. For the pure SnO_2 nanoparticles and functionalized P(Asn-co-Phe)/SnO_2 nanoparticles, TEM examination was performed (JEOL: JEM 2100) at voltage of 200 kV.

2.4 Electrochemical studies

Electrochemical tests employing three electrode systems immersed in 0.1 mol/L HCl were used to analyse the corrosion behaviour of pure epoxy resin, EP−SnO_2, EP−P(Asn-co-Phe), and EP−P(Asn-co-Phe)/SnO_2 coated tinplate. 0.1 mol/L HCl was utilised as the electrolyte. The coated specimens serve as the working electrode, the reference electrode is silver/silver chloride (Ag/AgCl), and the counter electrode is platinum. Electrochemical impedance spectroscopy (EIS) was used to examine the electrochemical properties of these coated specimens utilising Autolab PGSTAT 30, Echo Chemie, B.V., and Netherlands. EIS investigations used a frequency range from 100 kHz to 10 mHz.

Pure epoxy resin, EP−SnO_2, EP−P(Asn-co-Phe), and EP−P(Asn-co-Phe)/SnO_2 coated tinplates were subjected to scanning electrochemical microscopy (SECM) measurements (CHI 920D SECM) in 0.1 mol/L HCl for various exposure time

(1, 24, 120, and 240 h). The ultramicroelectrode (UME) tip was used for this approach. UME monitored the redox activity of the solid/liquid interface. The UME in this experiment was a platinum microelectrode with a diameter of 20 μm. The reference, counter, and working electrodes were Ag/AgCl, Pt strip, and coated surface, respectively. The scratched coated surface was used for SECM mapping. The potential of ±0.250 V was used from the φ_{corr} to carry out the polarization studies with the scan rate of 10 mV/min. To confirm that the results were repeatable, all electrochemical measurements were carried out in triplicate.

2.5 Morphological investigations

SEM/EDX analysis was used to examine the surface morphological structures and elemental composition of EP, EP−SnO_2, EP−P(Asn-co-Phe), and EP−P(Asn-co-Phe)/SnO_2 coated tinplate after 240 h of immersion in 0.1 mol/L HCl (Model JSM−7610F). After 240 h of immersion in 0.1 mol/L HCl, XRD tests were carried out on the EP, EP−SnO_2, EP−P(Asn-co-Phe), and EP−P(Asn-co-Phe)/SnO_2 coated tinplate (Siemens D5000 X-ray diffractometer).

2.6 Mechanical properties

The bonding strength of EP, EP−SnO_2, EP−P(Asn-co-Phe), and EP−P(Asn-co-Phe)/SnO_2 coated tinplate was examined before and after immersion in 0.1 mol/L HCl using the pull-off adhesion test as per ASTM D4541 standard utilising the testing equipment (Instron). To obtain reliable results, the trials were repeated three times. The microhardness was investigated using the HM113 Vickers hardness tester. To obtain reliable results, five measurements were made for EP, EP−SnO_2, EP−P(Asn-co-Phe), and EP−P(Asn-co-Phe)/SnO_2 coated tinplate. Before and after immersion in 0.1 mol/L HCl, the tensile strength of EP, EP−SnO_2, EP−P(Asn-co-Phe), and EP−P(Asn-co-Phe)/SnO_2 coated tinplate was tested using the universal testing equipment.

2.7 Permeability of O_2 and H_2O

The pervaporation test was used to investigate the water permeability of EP, EP−SnO_2, EP−P(Asn-co-Phe), and EP−P(Asn-co-Phe)/SnO_2 nanocomposite coated tinplates before and after exposure to 0.1 mol/L HCl for various time. According to ASTM D4491, water permeability was determined by measuring the mass of water passing through the film throughout the exposure time, which ranged from 1 to 240 h. In addition, the oxygen permeability of the coated tinplate was tested according to ASTM D3985.

2.8 Antimicrobial activity assay

Using the agar well diffusion method, the antibacterial activity of EP−P(Asn-co-Phe)/SnO_2 nanocomposite against bacteria pathogens was examined. Agar is a nutrient that is used to cultivate bacteria. The germs were acquired from King Institute of Preventive Medicine and Research, Guindy, Chennai, Tamil Nadu, India. During this study, two GNB (*E. coli* and *P. aeruginosa*) and one GPB (*S. aureus*) microorganisms were employed. The overnight bacterial culture was dissolved in freshly prepared agar medium, which was then put into sterilised petri dishes and allowed to solidify. This procedure was carried out in a laminar flow at room temperature, and wells with a diameter of 5 mm were created in each plate using a sterile micropipette tip, with a sterilised needle used to remove the agar plug. Each stock suspension of EP−P(Asn-co-Phe)/SnO_2 nanocomposite was made and placed into each well and incubated at 37 °C overnight. The activity of EP−P(Asn-co-Phe)/SnO_2 nanocomposite was determined after 24 h by measuring the inhibitory zone around each well.

3 Results and discussion

3.1 Investigation of modified SnO_2

3.1.1 TGA/DSC

In order to understand the thermal behaviour and interaction between the polymer and SnO_2 nanoparticles of the prepared P(Asn-co-Phe)/SnO_2 composite, the TGA analysis was carried out and the results are displayed in Fig. 1. From the TGA analysis, the thermal degradation of SnO_2 nanoparticles occurred with the mass loss of 15% and 60% with initial degradation at 100 °C and final decomposition at 210 °C. The initial degradation is because of the evolution of water and low molecular mass oligomers. In the case of P(Asn-co-Phe)/SnO_2, films show an increased thermal stability compared to the pure SnO_2 nanoparticles. The P(Asn-co-Phe)/SnO_2 nanocomposite shows the initial degradation temperature at 270 °C

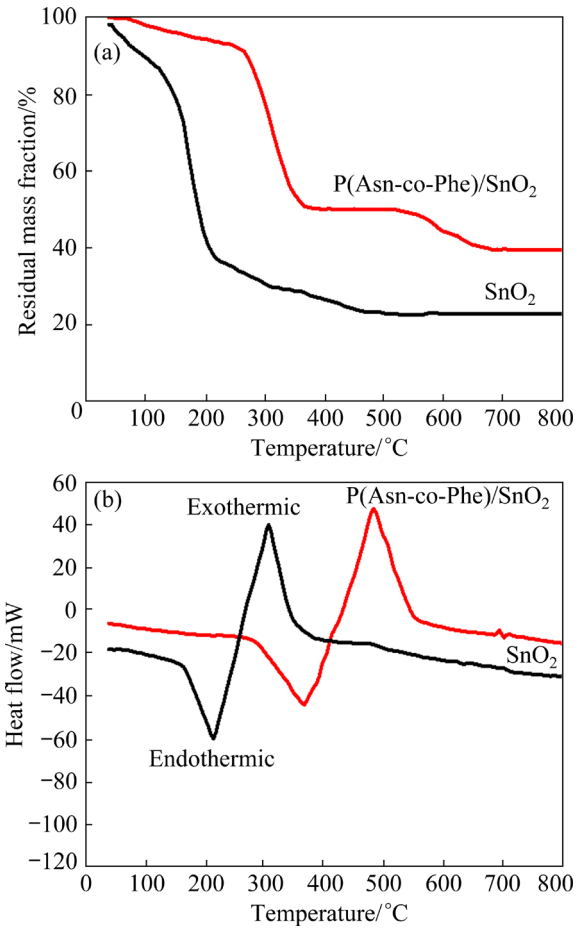

Fig. 1 TGA (a) and DSC (b) curves for pure SnO_2 nanoparticles and P(Asn-co-Phe)/SnO_2 nanoparticles

with 10% mass loss and final degradation temperature is around 370 °C with 50% mass loss, and this is reasonably higher compared to the pure SnO_2 nanoparticles, due to high thermal properties of SnO_2 in the polymer matrixes. DSC results are shown in Fig. 1 for SnO_2 nanoparticles and P(Asn-co-Phe)/SnO_2 nanocomposite samples. An endothermic peak for SnO_2 nanoparticles is observed at 200 °C and exothermic peak at 42 °C. For P(Asn-co-Phe)/SnO_2 nanocomposites, endothermic peak is observed at 380 °C and exothermic peak at 480 °C. The endothermic peak refers to the evaporation of water in the sample. The exothermic peak is related to the decomposition of the products.

3.1.2 XRD

The XRD patterns of SnO_2 and P(Asn-co-Phe) are presented in Fig. S1 of Supplementary Material. It is seen that the nanocrystalline peaks are observed at (2θ) 25.72°, 35.30°, 37.94°, 52.70°, 57.66°, 61.44°, 66.66°, and 77.0° for pure SnO_2 nanoparticles, which are related, respectively, by their indices (110), (101), (200), (211), (220), (310), (301) and (321) corresponding to typical tetragonal type of SnO_2 (JCPDS data card 71-0652) [29]. The XRD pattern of P(Asn-co-Phe)/SnO_2 nanocomposite shows slight shift from their respective standard positions due to P(Asn-co-Phe) matrix. However, the intensities of the peaks are reduced to some extent. This indicates the presence of SnO_2 and suggests that there is a kind of interaction between P(Asn-co-Phe) and SnO_2 nanoparticles which lead to the non-destruction of SnO_2 nanoparticles [30].

3.1.3 FTIR

The FTIR spectra of SnO_2 nanoparticles are shown in Fig. 2, with a broad band ranging from 3481 to 3280 cm^{-1} and a smaller peak at 1638 cm^{-1} ascribed to the O—H moiety's stretch and bend vibrational mode. The Sn—O vibration in lattice structures causes the peak in the region of 1587−921 cm^{-1}. Because of the homogeneity of two peaks at 685 and 537 cm^{-1} that are assigned to vibrational mode of Sn—O—Sn and Sn—O, respectively, the wide range bands at 770−423 cm^{-1}

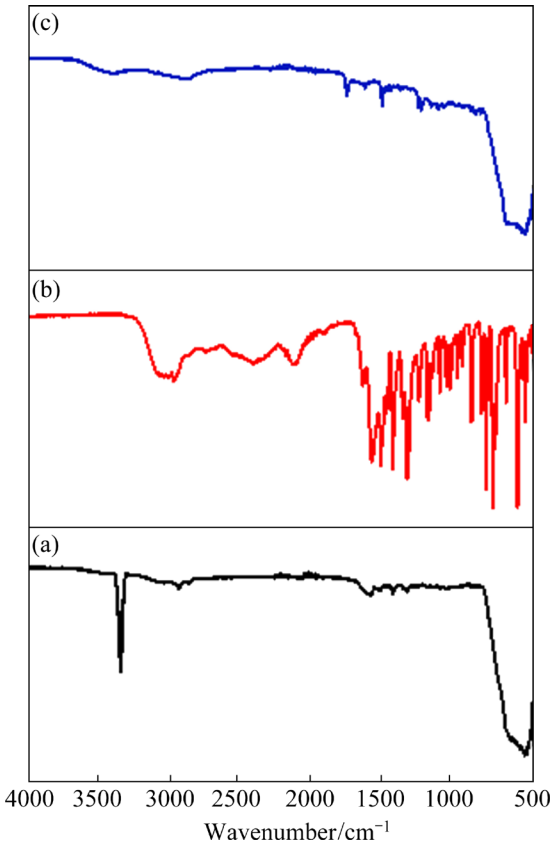

Fig. 2 FTIR spectra of pure SnO_2 nanoparticles (a), P(Asn-co-Phe) (b) and P(Asn-co-Phe)/SnO_2 (c)

exist. The N—H bending vibration (amide II) band at 1543 cm^{-1} and the C═O stretching vibration (amide I) band with a maximum at 1657−1649 cm^{-1} and a shoulder at 1719 cm^{-1} identifies the helical secondary conformation of polypeptide chain. The appearance of a prominent shoulder of amide I at 1617 cm^{-1} demonstrates the presence of sheet structures. The resulting product, P(Asn-co-Phe)/SnO_2, has peaks at 1728, 1475, and 1209 cm^{-1} when SnO_2 nanoparticles are functionalized with P(Asn-co-Phe). The broad peak at 763−426 cm^{-1} can also be seen in the wide range bands. The functionalization of SnO_2 by P(Asn-co-Phe) is confirmed by these peaks.

3.1.4 AFM

Figure 3 shows the typical AFM images for pure SnO_2 nanoparticles and P(Asn-co-Phe)/SnO_2 nanoparticles. The AFM image of SnO_2 nanoparticles shows smooth topographic features, whereas the image of P(Asn-co-Phe)/SnO_2 nanoparticles shows rough surface morphology. For pure SnO_2 nanoparticles, the size is found to be 60 nm, whereas for P(Asn-co-Phe)/SnO_2 nanoparticles, the size is observed to be 80 nm. The increase in the size and the surface area of P(Asn-co-Phe)/SnO_2 nanoparticles shows the functionalization of SnO_2 with P(Asn-co-Phe).

3.1.5 SEM/EDX

The SEM images of SnO_2 nanoparticles and P(Asn-co-Phe)/SnO_2 nanoparticles are depicted in Figs. 4(a, c). Figure 4(a) shows the agglomerated spherical structure of SnO_2 nanoparticles of 60 nm. Figure 4(c) shows the well-dispersed SnO_2 nanoparticles in the polymer matrix. The elements

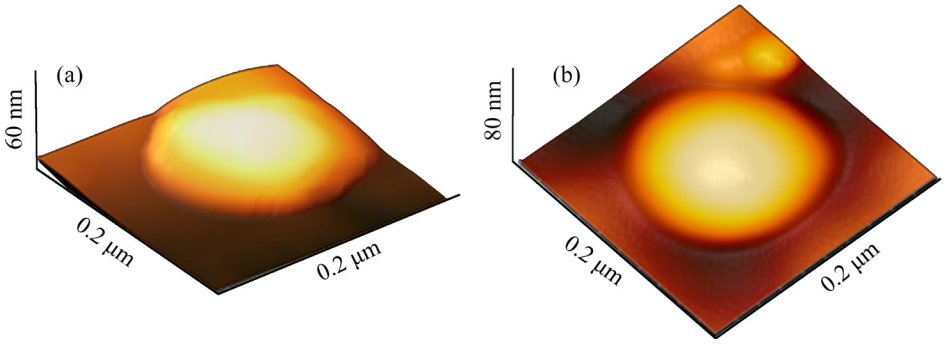

Fig. 3 AFM images for pure SnO_2 nanoparticles (a) and P(Asn-co-Phe)/SnO_2 (b) nanoparticles

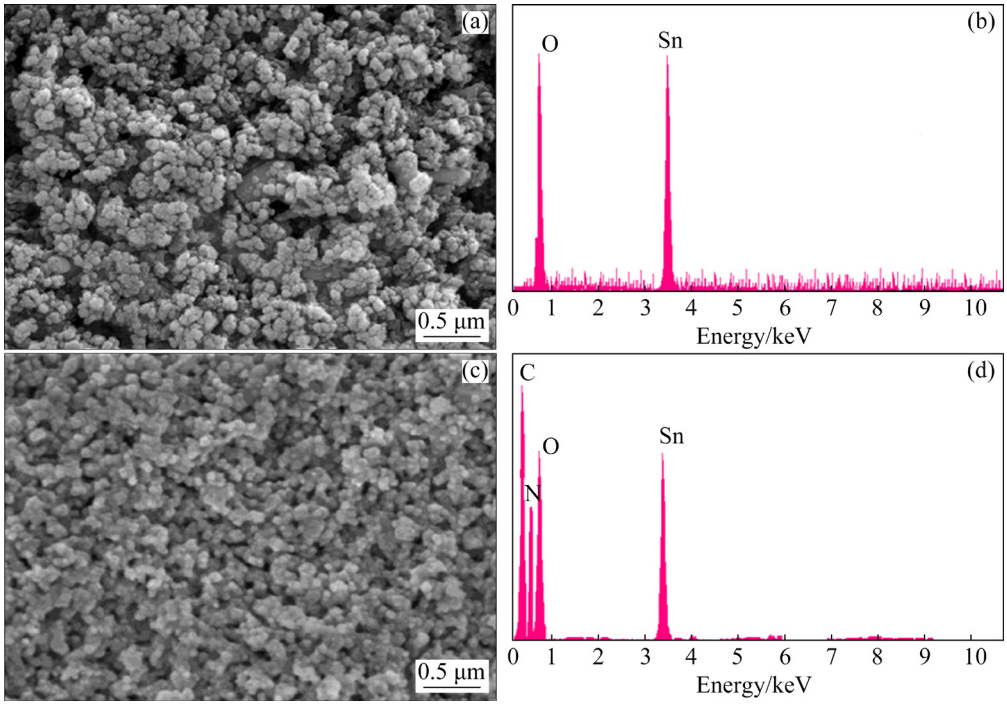

Fig. 4 SEM/EDX results of pure SnO_2 nanoparticles (a, b), and P(Asn-co-Phe)/SnO_2 nanoparticles (c, d)

present in the SnO_2 nanoparticles and P(Asn-co-Phe)/SnO_2 nanoparticles are shown in Figs. 4(b, d), respectively. It is confirmed from the EDX analysis, that the SnO_2 nanoparticles consist of stannum and oxygen only, whereas P(Asn-co-Phe)/SnO_2 nanoparticles consist of C, N, Sn and O. Therefore, it is confirmed that the SnO_2 nanoparticles are modified by P(Asn-co-Phe) [31].

3.1.6 TEM

TEM has been utilized to further investigate the morphologies and crystalline structure of the P(Asn-co-Phe)/SnO_2 nanoparticles. Figures 5(a, b) show the TEM images of pure SnO_2 nanoparticles and P(Asn-co-Phe)/SnO_2 nanoparticles. The image in Fig. 5(a) shows that the particles are in nano meter range and are agglomerated. The image clearly shows the crystalline nature of the pure SnO_2 nanoparticles. It is observed from Fig. 5(b) that the SnO_2 nanoparticle is uniformly dispersed in polymer matrix. The distribution pattern between SnO_2 nanoparticles and the polymer shows that the SnO_2 nanoparticles are encapsulated by P(Asn-co-Phe), which confirms the uniform distribution of nanoparticles into the polymer matrix [32].

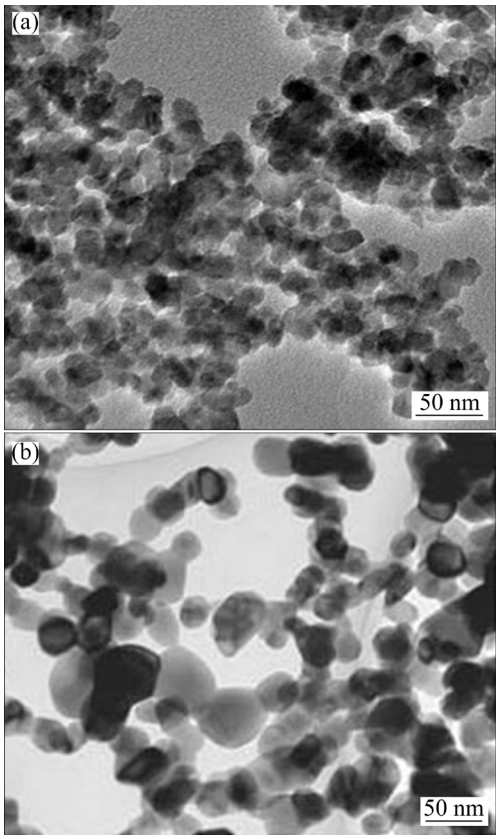

Fig. 5 TEM images of pure SnO_2 nanoparticles (a) and P(Asn-co-Phe)/SnO_2 nanoparticles (b)

3.2 Electrochemical investigation

3.2.1 Electrochemical impedance spectroscopy

Figure S2 in Supplementary Material displays the Nyquist plots for tinplate, pure epoxy and different mass fractions of P(Asn-co-Phe)/SnO_2 nanoparticles in the epoxy coating on tinplate immersed in 0.1 mol/L HCl. The coating resistance increases sharply by the addition of 4 wt.% SnO_2 nanoparticles to the epoxy. Introduction of SnO_2 nanoparticles beyond 4 wt.% to epoxy coating decreases the coating resistance. From this, it is observed that, the optimal content of SnO_2 nanoparticles is found to be 4 wt.%. Beyond 4 wt.%, there is a decrease in the coating resistance. This may be due to the improper and nonuniform dispersion of SnO_2 nanoparticles at higher content. Figures 6(a−d) depict the Nyquist plots of EP, EP−SnO_2, EP−P(Asn-co-Phe) and EP−P(Asn-co-Phe)/SnO_2 nanocomposite coating on tinplate immersed in 0.1 mol/L HCl for 1, 24, 120 and 240 h, respectively. It is observed that impedance decreases with increase in exposure time. The highest impedance is observed for EP−P(Asn-co-Phe)/SnO_2 nanocomposite coatings. The improved impedance in EP−P(Asn-co-Phe)/SnO_2 composite may be due to the reduced passageways of 0.1 mol/L HCl solution into the coating/tinplate interface in the presence of P(Asn-co-Phe)/SnO_2 nanoparticles. From this observation, it is suggested that the EP−P(Asn-co-Phe)/SnO_2 nanocomposite film displays superior barrier properties against corrosion. Figure S3 in Supplementary Material shows the equivalent electrical circuit diagrams for EP, EP−SnO_2, EP−P(Asn-co-Phe) and EP−P(Asn-co-Phe)/SnO_2 nanocomposite coating on tinplate immersed in 0.1 mol/L HCl for 1, 24, 120 and 240 h. The components of the coated tinplate are solution resistance (R_s), charge transfer resistance (R_{ct}), coating resistance (R_{coat}), constant phase element as the double layer capacitance (CPE_{dl}) and constant phase element of coating (CPE_{coat}).

Table 1 displays electrochemical parameters obtained after fitting the Nyquist plots. The R_{ct} values of the epoxy, EP−SnO_2, EP−P(Asn-co-Phe) and EP−P(Asn-co-Phe)/SnO_2 nanocomposite coatings are found to be 109.99, 1364.70, 1675.17, and 3985.12 kΩ·cm^2, respectively, compared to bare tinplate (35.12 kΩ·cm^2) for 1 h immersion in 0.1 mol/L HCl solution. However, the R_{ct} value of EP−P(Asn-co-Phe)/SnO_2 nanocomposite gets very

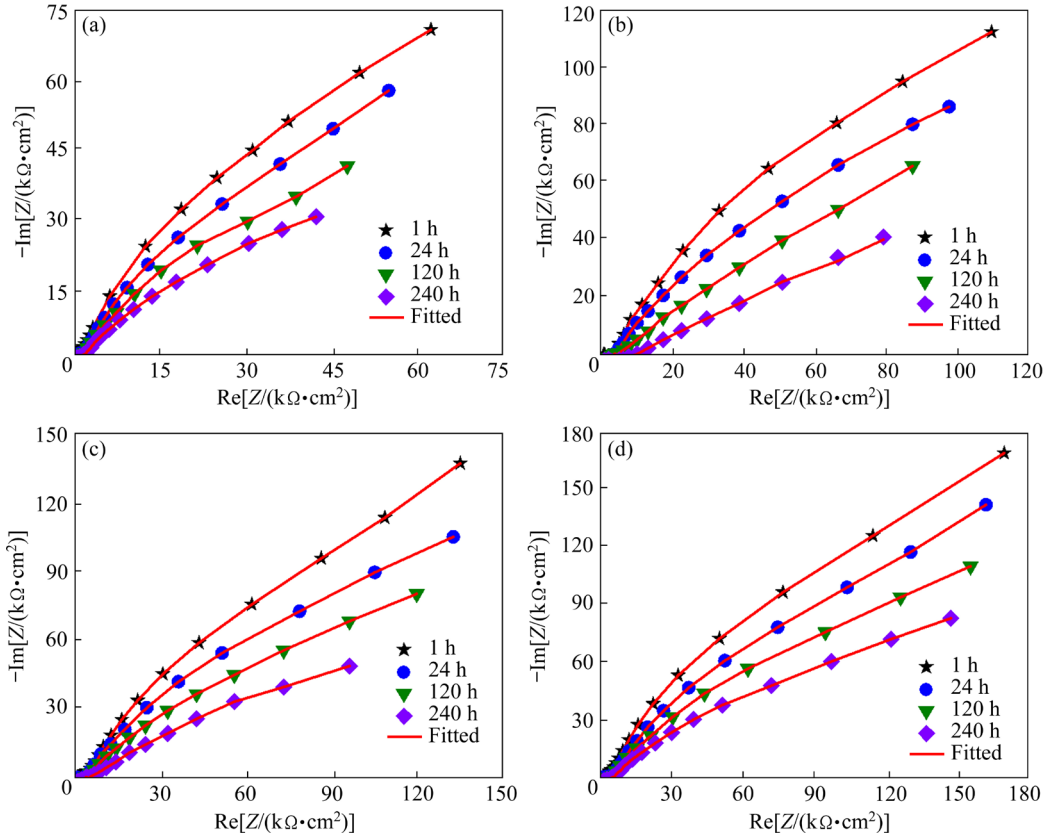

Fig. 6 Nyquist plots of pure epoxy resin (EP) (a), EP−SnO_2 (b), EP−P(Asn-co-Phe) (c) and EP−P(Asn-co-Phe)/SnO_2 (d) nanocomposite coating on tinplate immersed in 0.1 mol/L HCl for 1, 24, 120 and 240 h

Table 1 Fitted results of EIS using equivalent circuit

Sample	Time/h	R_s/ ($\Omega\cdot cm^2$)	R_{coat}/ ($k\Omega\cdot cm^2$)	CPE_c/ ($\mu F\cdot s^{n_c-1}\cdot cm^{-2}$)	n_c	R_{ct}/ ($k\Omega\cdot cm^2$)	CPE_{dl}/ ($\mu F\cdot s^{n_{dl}-1}\cdot cm^{-2}$)	n_{dl}
Bare tinplate	1	105	–	–	–	35.12	387.45	0.63
	24	90	–	–	–	21.45	678.50	0.60
	120	71	–	–	–	11.65	998.90	0.57
	240	60	–	–	–	0.12	1205.35	0.54
Epoxy (EP) coating	1	119	101.41	52.15	0.70	109.97	310.41	0.74
	24	107	82.78	91.23	0.68	93.12	546.70	0.72
	120	98	55..39	111.38	0.66	62.76	712.34	0.70
	240	87	01.03	143.25	0.64	02.80	904.25	0.68
EP−SnO_2 coating	1	129	1211.44	60.24	0.74	1364.70	276.78	0.80
	24	121	1074.98	111.67	0.72	1178.65	556.40	0.78
	120	114	878.45	131.23	0.70	908.43	678.90	0.76
	240	109	686.30	155.70	0.68	701.90	798.15	0.74
EP−P(Asn-co-Phe) coating	1	141	1368.90	70.95	0.78	1475.17	256.12	0.84
	24	135	1145.75	85.71	0.76	1258.56	417.40	0.82
	120	128	941.24	100.78	0.74	1076.43	608.75	0.80
	240	119	723.17	120.09	0.72	898.35	751.17	0.78
EP−P(Asn-co-Phe)/ SnO_2 coating	1	178	3854.70	88.66	0.84	3985.12	218.19	0.88
	24	161	3779.19	120.97	0.83	3875.70	325.56	0.87
	120	143	3659.25	148.80	0.82	3797.45	476.97	086
	240	131	3565.75	254.17	0.81	3699.42	512.45	0.85

slowly decreased to 3699.42 kΩ·cm^2 compared to the EP−SnO_2 (701.90 kΩ·cm^2), and EP−P(Asn−co−Phe) (898.35 kΩ·cm^2) coating for 240 h immersion in 0.1 mol/L HCl. This is because of the hard dense layer of P(Asn-co-Phe)/SnO_2 nanoparticles formed at the polymer interface matrix, which helps to enhance the better corrosion protection performance of the composite coating on tinplate [33].

The coating resistance values of tinplate coated with EP, EP−SnO_2, EP−P(Asn-co-Phe) and EP−P(Asn-co-Phe)/SnO_2 nanocomposite are 101.41, 1211.44, 1568.90 and 3854.70 kΩ·cm^2, respectively, for 1 h immersion in 0.1 mol/L HCl. However, very slow decrease in the coating resistance is observed for tinplate coated with EP−P(Asn-co-Phe)/ SnO_2 (3565.75 kΩ·cm^2) compared to EP−SnO_2 (386.30 kΩ·cm^2), and EP−P(Asn-co-Phe) (723.17 kΩ·cm^2) for 240 h immersion in 0.1 mol/L HCl solution. Pure epoxy displays much lower coating resistance compared to EP−P(Asn-co-Phe)/SnO_2 nanocomposite coatings on tinplate. Higher coating resistance of EP−P(Asn-co-Phe)/SnO_2 indicates the superior anti-corrosion ability of the coatings. The improved values of coating and charge transfer resistances are shown by EP−P(Asn-co-Phe)/SnO_2, which results from good dispersion of P(Asn-co-Phe)/SnO_2 nanoparticles in polymer matrix which prevents the degradation of the coating against corrosive ions.

3.2.2 Potentiodynamic polarization studies

Figure 7 demonstrates the polarization curves of EP, EP−SnO_2, EP−P(Asn-co-Phe) and EP−P(Asn-co-Phe)/SnO_2 nanocomposite coating on tinplate immersed in 0.1 mol/L HCl for 1, 24, 120 and 240 h, respectively. The resultant plots are extrapolated and the data are displayed in Table 2. The analysis of the data shows that the steel specimen coated with EP−P(Asn-co-Phe)/SnO_2 nanocomposite exhibits reduced current density (J_{corr}) due to corrosion and least corrosion rate (CR). However, enhanced values of J_{corr} and CR are obtained for the plain PU coated specimen. This confirms the improved barrier properties of the EP−P(Asn-co-Phe)/SnO_2 coated specimen due to the effective reaction between highly reactive

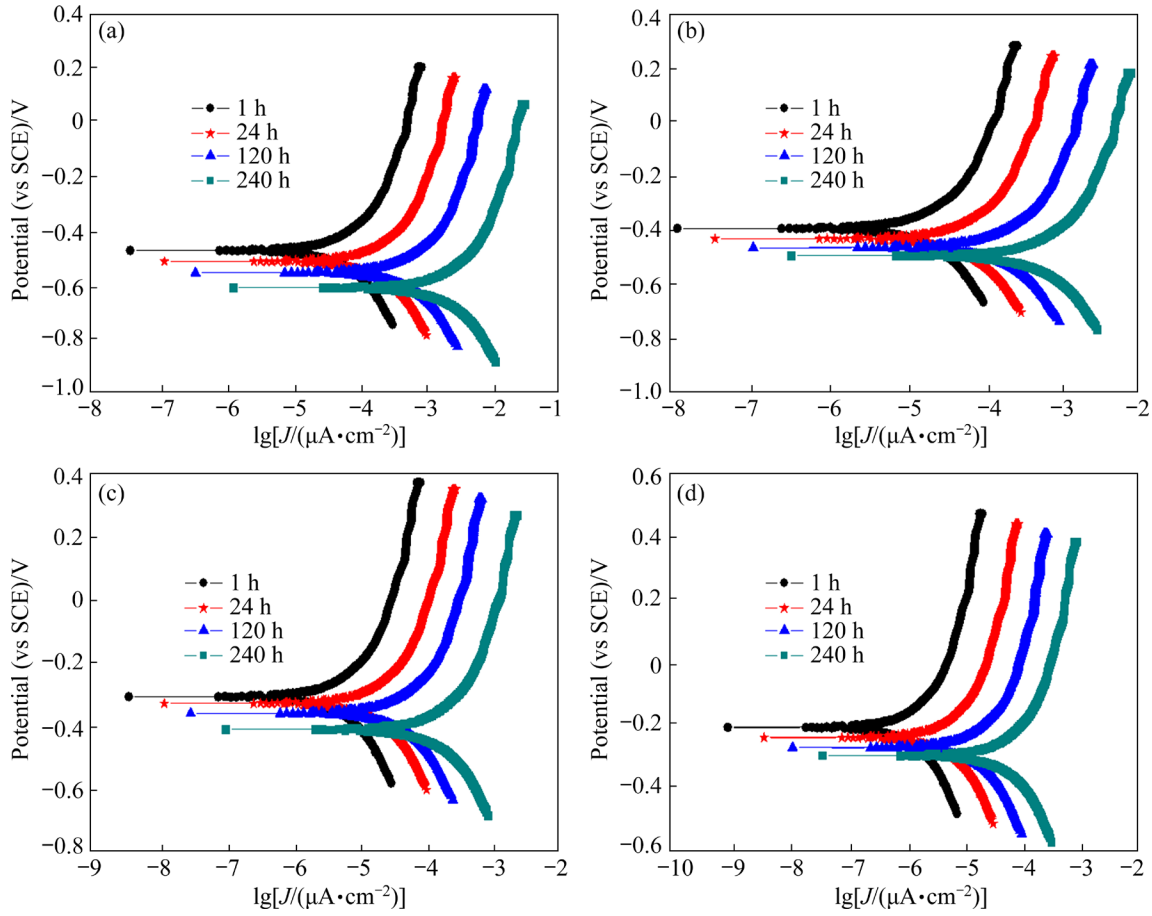

Fig. 7 Potentiodynamic polarization curves of pure epoxy resin (EP) (a), EP−SnO_2 (b), EP−P(Asn-co-Phe) (c) and EP−P(Asn-co-Phe)/SnO_2 (d) nanocomposite coating on tinplate immersed in 0.1 mol/L HCl for 1, 24, 120 and 240 h

Table 2 Results of potentiodynamic polarization measurements

Sample	Time/h	φ_{corr}/mV	J_{corr}/(μA·cm^{-2})	R_p/(kΩ·cm^2)	CR/(mm·a^{-1})
Bare tinplate	1	−597	61.25	35.56	0.9998
	24	−721	78.06	21.21	1.9942
	120	−846	96.14	11.65	3.1054
	240	−970	117.55	0.13	5.4897
Epoxy (EP) coating	1	−402	18.02	211.80	0.2264
	24	−446	22.88	176.15	0.2485
	120	−501	31.00	118.53	0.2673
	240	−567	46.87	3.92	0.2819
EP−SnO_2 coating	1	−306	8.25	2576.27	0.1645
	24	−350	15.34	2253.75	0.1809
	120	−403	22.34	1786.99	0.2022
	240	−446	29.15	1388.31	0.2212
EP−P(Asn-co-Phe) coating	1	−197	3.28	2844.21	0.1452
	24	−245	5.45	2404.45	0.1645
	120	−300	7.92	2017.80	0.1812
	240	−346	9.12	1621.52	0.2018
EP−P(Asn-co-Phe)/SnO_2 coating	1	−103	1.05	7840.53	0.0070
	24	−116	1.28	7655.63	0.0084
	120	−135	1.42	7456.81	0.0102
	240	−157	1.65	7264.78	0.0126

nanoparticles (P(Asn-co-Phe)/SnO_2) and epoxy matrix. The values of J_{corr} for bare steel, EP, EP−SnO_2, EP−P(Asn-co-Phe) and EP−P(Asn-co-Phe)/SnO_2 coated specimens are found to be 61.25, 18.02, 8.25, 3.28 and 1.05 μA/cm^2, respectively, when these specimens are in contact with the electrolyte for 1 h. However, these values of J_{corr} for bare steel, EP, EP−SnO_2, EP−P(Asn-co-Phe) and EP−P(Asn-co-Phe)/SnO_2 coated specimens are increased to 117.55, 46.87, 29.15, 9.12 and 1.65 μA/cm^2, respectively, when these specimens are in contact with the chloride media for longer time (240 h). Moreover, higher R_p and lower corrosion rate (CR) values are obtained for bare steel (R_p: 35.56 kΩ·cm^2 and CR: 0.9998 mm/a), EP (R_p: 211.80 kΩ·cm^2 and CR: 0.2264 mm/a), EP−SnO_2 (R_p: 2576.27 kΩ·cm^2 and CR: 0.1809 mm/a), EP−P(Asn-co-Phe) (R_p: 2844.21 kΩ·cm^2 and CR: 0.1452 mm/a), and EP−P(Asn-co-Phe)/SnO_2 (R_p: 7840.53 kΩ·cm^2 and CR: 0.0074 mm/a) coated specimens at 1 h. The values of CR and R_p for EP−P(Asn-co-Phe)/SnO_2 coated specimen are slightly changed (R_p: 7264.78 kΩ·cm^2 and CR: 0.0126 mm/a) even when they are in contact with the electrolyte for the longer period (240 h).

These results show that the addition of P(Asn-co-Phe)/SnO_2 nanoparticles to the epoxy matrix improves drastically when it is compared with other investigated coatings such as EP, EP−SnO_2, and EP−P(Asn-co-Phe). The reactive P(Asn-co-Phe)/SnO_2 nanoparticles help to form a uniform and compact coating due to the cross-linking structures which impede the movement of ions towards metal−coating interface. However, drastic degradation of pure epoxy coated specimen is noticed even during the short period of exposure to the electrolytes. On the other hand, EP−P(Asn-co-Phe)/SnO_2 coated specimen shows least degradation behavior even after prolonged contact with the electrolytes, thus improving the life span of the coated specimen.

3.2.3 SECM studies

Figure 8 shows SECM measurements of EP, EP−SnO_2, EP−P(Asn-co-Phe) and EP−P(Asn-co-

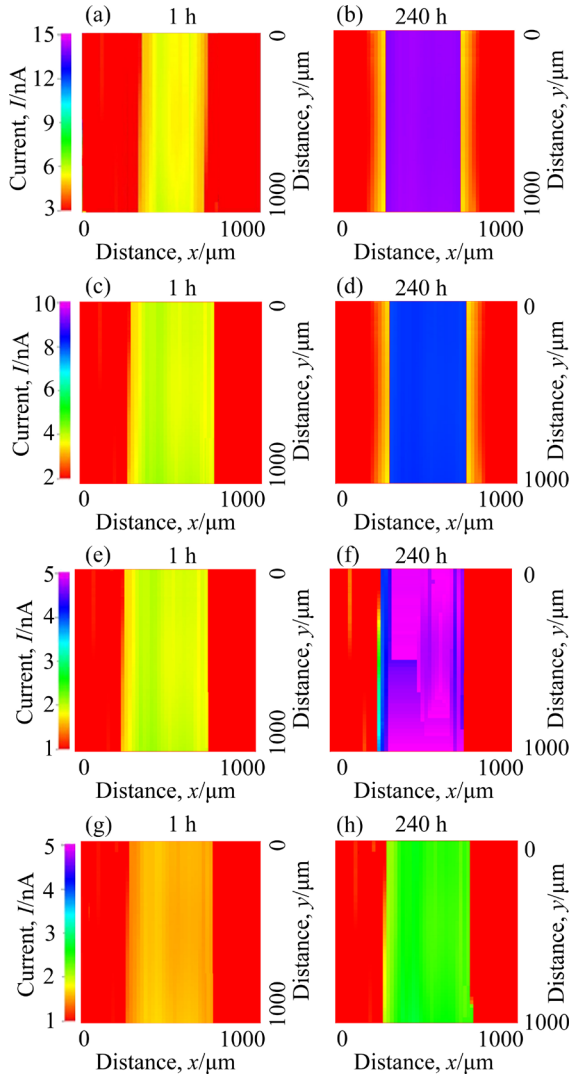

Fig. 8 SECM results of pure EP (a, b), EP−SnO_2 (c, d), EP−P(Asn-co-Phe) (e, f) and EP−P(Asn-co-Phe)/SnO_2 (g, h) nanocomposite coating on tinplate immersed in 0.1 mol/L HCl for 1, and 240 h at tip potential of +0.60 V vs Ag/AgCl/KCl reference electrode for detection of ferrous ions

Phe)/SnO_2 nanocomposite coating on tinplate for 1 and 240 h at +0.60 V in 0.1 mol/L HCl [34]. The highest current at the defects is due to the oxidation of ferrous ions. The epoxy coated tinplate shows 5.7 nA for 1 h whereas the current for 240 h is 14.9 nA. This increase in current on exposure with time is due to the oxidation of Fe^{2+} to Fe^{3+} ions. The resulting currents at the scratched EP−SnO_2, EP−P(Asn-co-Phe) and EP−P(Asn-co-Phe)/SnO_2 coated tinplate for 1 h immersion in 0.1 mol/L HCl solution are 3.8, 2.0 and 1.5 nA, respectively. However, the currents at the scratched EP−SnO_2, EP−P(Asn-co-Phe) and EP−P(Asn-co-Phe)/SnO_2 coated tinplate for 240 h immersion in 0.1 mol/L HCl solution are 9.0, 5.1 and 2.8 nA, respectively. It is observed that EP−P(Asn-co-Phe)/SnO_2 coated tinplate shows less current distribution at the scratched coated surface due to less dissolution of Fe^{2+} ions.

Figure 9 depicts the SECM measurements of neat EP, EP−SnO_2, EP−P(Asn-co-Phe) and EP−P(Asn-co-Phe)/SnO_2 nanocomposite coating on tinplate for 1 h and 240 h at +0.17 V in 0.1 mol/L HCl solution. The highest current at the defects is due to the formation of stannous ions. The epoxy coated tinplate shows 14.8 nA for 1 h whereas the current for 240 h is 24.9 nA. The rate of increased

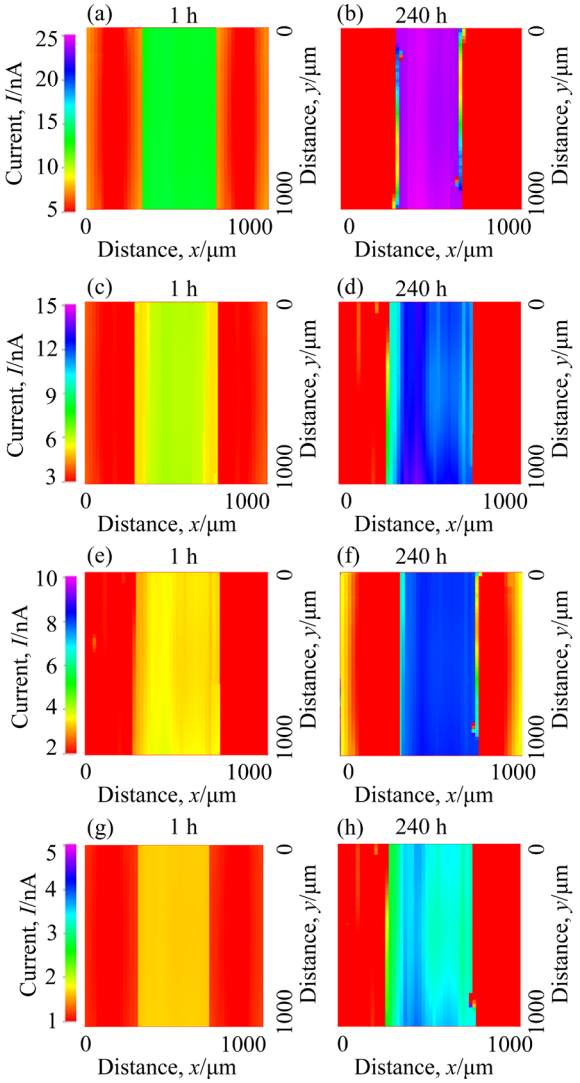

Fig. 9 SECM results of pure EP (a, b), EP−SnO_2 (c, d), EP−P(Asn-co-Phe) (e, f) and EP−P(Asn-co-Phe)/SnO_2 (g, h) nanocomposite coating on tinplate immersed in 0.1 mol/L HCl for 1 and 240 h at tip potential of +0.17 V vs Ag/AgCl/KCl reference electrode for detection of stannous ions

dissolution of tinplate with increase in the contact time with the electrolyte is due to the oxidation of Sn^{2+} ions to Sn^{4+} ions. The resultant currents detected at the defects of EP−SnO_2, EP−P(Asn-co-Phe) and EP−P(Asn-co-Phe)/SnO_2 coated tinplate for 1 h immersion in 0.1 mol/L HCl solution are 5.9, 3.8 and 1.8 nA, respectively. However, the currents detected at the defects of EP−SnO_2, EP−P(Asn-co-Phe) and EP−P(Asn-co-Phe)/SnO_2 coated tinplate for 240 h immersion in 0.1 mol/L HCl solution are 12.1, 8.5 and 3.5 nA, respectively. It is observed that the EP−P(Asn-co-Phe)/SnO_2 coated tinplate shows less current distribution of 1.8 and 3.5 nA, respectively. In both cases, for the coated samples at tip potential of +0.60 and +0.17 V, the current increases with increasing the immersion time. Moreover, a lower tip current observed at the scratch of EP−SnO_2, EP−P(Asn-co-Phe) and EP−P(Asn-co-Phe)/SnO_2 coated tinplate results in the development of passive layer [35]. The passive layer formation prevents the dissolution of tinplate. Hence, the incorporation of P(Asn-co-Phe)/SnO_2 nanoparticles in epoxy matrix enhances the tinplate resistance against corrosion. Hence, the SECM studies show that the inclusion of P(Asn-co-Phe)/SnO_2 in the epoxy coating on tinplate enhances the protection of tinplate due to the presence of N and adsorption of amino acids on the active corrosion sites of the metal sites [36].

The peak currents (I_{peak}) at +0.60 and +0.17 V (vs Ag/AgCl/saturated KCl) are calculated for the detection of ferrous and stannous ions from Figs. 8 and 9 according to the line scan analysis, as shown in Fig. S4(a, b) in Supplementary Material, respectively. From Fig. S4(a), I_{peak} due to the detection of ferrous ions is higher for EP coated specimen (14.9 nA/cm^2) than that of EP−P(Asn-co-Phe)/SnO_2 coated tinplate (2.8 nA) after 240 h. There is a sharp increase in I_{peak} for the pure epoxy coated specimen with test time due to the increase in the dissolution of Fe. On the other hand, there is slow increase in I_{peak} for EP−P(Asn-co-Phe)/SnO_2 coated tinplate with test time due to the formation of corrosion products at the scratch which decrease the further dissolution of Fe. However, from Fig. S4(b), I_{peak} due to the detection of stannous ions is found to be much higher for EP coated specimen (24.9 nA) than that of EP−P(Asn-co-Phe)/SnO_2 coated tinplate (3.5 nA) after 240 h. There is a sharp increase in I_{peak} for the pure epoxy coated specimen with test time due to the increase in the dissolution of stannum. On the other hand, there is slow increase in I_{peak} for EP−P(Asn-co-Phe)/SnO_2 coated tinplate with test time due to the formation of corrosion products at the scratch which decrease the further dissolution of Sn. From this analysis, it is concluded that the rate of corrosion of the EP coating is much higher than that of the EP−P(Asn-co-Phe)/SnO_2 coated tinplate due to increased dissolution of Fe and Sn at prolonged exposure to the electrolyte.

3.3 Water contact angle measurements

Water contact angle measurements were carried out in order to get information about the investigated coatings whether they are hydrophilic or hydrophobic. Hydrophobic property confirms the barrier abilities of the coatings. Figure 10 presents water contact angle measurements on pure EP, EP−SnO_2, EP−P(Asn-co-Phe) and EP−P(Asn-co-Phe)/SnO_2 coating surfaces. The contact angles on pure EP, EP−SnO_2, EP−P(Asn-co-Phe) and EP−P(Asn-co-Phe)/SnO_2 are found to be 75°, 95°, 102°, and 133°, respectively. The surface is said to be hydrophilic if the angle value is less than 90°, and if the value is greater than 90°, it is said to be hydrophobic [37,38]. The EP−SnO_2, EP−P(Asn-co-Phe) and EP−P(Asn-co-Phe)/SnO_2 coated surfaces are found to be hydrophobic. However, the EP−P(Asn-co-Phe)/SnO_2 coated surface shows superior hydrophobic property, which demonstrates superior barrier properties among the investigated sample coatings. These results compliment other results of the investigated coatings.

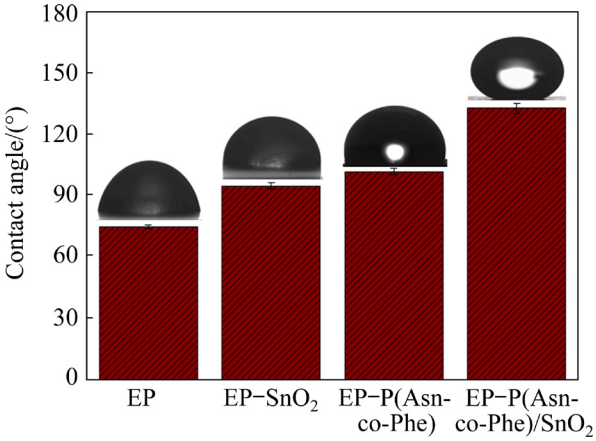

Fig. 10 Water contact angle on pure epoxy resin (EP), EP−SnO_2, EP−P(Asn-co-Phe) and EP−P(Asn-co-Phe)/SnO_2 nanocomposite coated tinplate surfaces

3.4 Surface morphological studies

3.4.1 SEM/EDX

Figure 11 depicts the SEM/EDX analyses of the cross-sectional area of EP, EP−SnO_2, EP−P(Asn-co-Phe) and EP−P(Asn-co-Phe)/SnO_2 nanocomposite coated tinplate after 240 h of immersion in 0.1 mol/L HCl. In the EP coating, the cracks/defects are highly visible. However, no significant cracks/pores are found for EP−SnO_2, EP−P(Asn-co-Phe) and EP−P(Asn-co-Phe)/SnO_2 nanocomposite coated tinplate. The P(Asn-co-Phe)/SnO_2 nanoparticles in the epoxy matrix help to block the aggressive ions reaching the bare part of the specimen. This suggests that the examined coated tinplate has improved corrosion resistance. The degradation products contain C, N, O, Sn, and increasing quantity of Fe, as evidenced by the EDX. EP−P(Asn-co-Phe)/SnO_2 nanocomposite coated tinplate has anticorrosion capabilities due to the production of complex oxides and chlorides of C, Sn, and Fe at scratch. As a result of the creation of stable adherent oxide layers at the coating/ tinplate

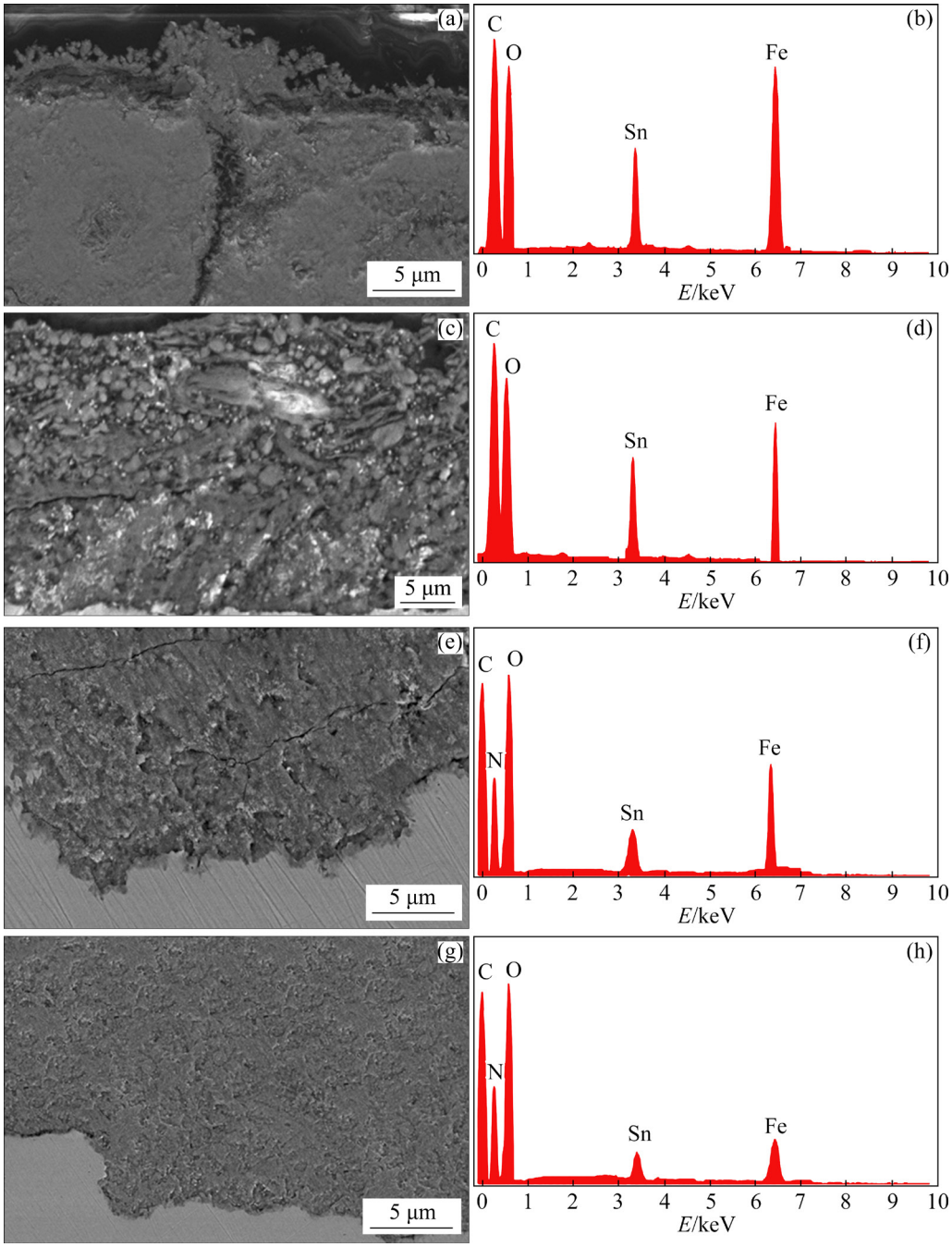

Fig. 11 SEM/EDX results of pure EP (a, b), EP−SnO_2 (c, d), EP−P(Asn-co-Phe) (e, f) and EP−P(Asn-co-Phe)/SnO_2 (g, h) nanocomposite coated tinplate after 240 h of immersion in 0.1 mol/L HCl

tinplate interface, the corrosion resistance of the investigated nanocomposite coated tinplate is improved. The presence of nitrogen in the P(Asn-co-Phe) helps to increase the adhesive strength and enhances the protective performance of EP−P(Asn-co-Phe)/SnO_2 nanocomposite.

3.4.2 XRD analysis of investigated coatings

Figure 12 shows the XRD patterns observed for the pure EP, EP−SnO_2, EP−P(Asn-co-Phe) and EP−P(Asn-co-Phe)/SnO_2 nanocomposite coated tinplate after 240 h of immersion in 0.1 mol/L HCl. The formation of degradation products after 240 h immersion of EP, EP−SnO_2, EP−P(Asn-co-Phe) and EP−P(Asn-co-Phe)/SnO_2 is clearly seen by the XRD investigation. From the analysis it is revealed that the corrosion products contain mainly SnO_2, Fe_3O_4 and γ-FeOOH. In EP−P(Asn-co-Phe)/SnO_2 after 240 h immersion, small peak formation of SnO_2 and Fe_3O_4 and enhanced peak of γ-FeOOH is observed. The creation of a tiny peak of Fe_3O_4 along with EP−P(Asn-co-Phe)/SnO_2 nanocomposite coatings over tinplate reveals that corrosion happens in a regulated manner. The tinplate coated with epoxy shows enhanced peak formation of γ-FeOOH. The intensity of the peak is higher for EP resin compared to that of EP−SnO_2, EP−P(Asn-co-Phe) and EP−P(Asn-co-Phe)/SnO_2 nanocomposites. The intensity of the peak is found to be reduced in EP−P(Asn-co-Phe)/SnO_2 due to the adsorption of SnO_2 nanoparticles. This research demonstrates that P(Asn-co-Phe) can be functionalized using SnO_2 nanoparticles.

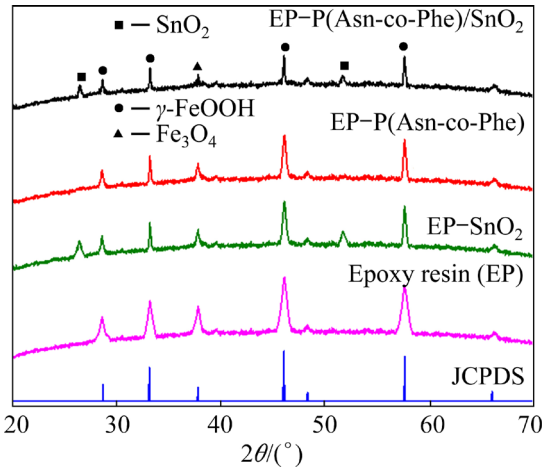

Fig. 12 XRD patterns for pure epoxy resin (EP), EP−SnO_2, EP−P(Asn-co-Phe) and EP−P(Asn-co-Phe)/SnO_2 nanocomposite coated tinplate after 240 h of immersion in 0.1 mol/L HCl

3.5 Mechanical properties of coated tinplate

The adhesion strength, hardness, and tensile strength of pure EP, EP−SnO_2, EP−P(Asn-co-Phe), and EP−P(Asn-co-Phe)/SnO_2 nanocomposite coated tinplate were measured before and after varied periods of immersion in 0.1 mol/L HCl. As a control, pure epoxy resin was employed in this experiment. The adhesion strength of pure EP, EP−SnO_2, EP−P(Asn-co-Phe) and EP−P(Asn-co-Phe)/SnO_2 before immersion is found to be 5.1, 7.2, 8.1 and 9.0 MPa, respectively, as shown in Fig. 13(a). After 240 h of immersion in 0.1 mol/L HCl, the adhesion strength of EP−SnO_2, EP−P(Asn-co-Phe), and EP−P(Asn-co-Phe)/SnO_2 nanocomposite is found to be 3.0, 4.0, and 7.0 MPa, respectively, in comparison to the pure epoxy coating adhesion strength of 1.0 MPa. Higher surface roughness and flexibility in the composite film are attributed to the doping of SnO_2 nanoparticles and epoxy resin into the polymer matrix, which improves the adhesion. The improved adhesion property of EP−P(Asn-co-Phe)/SnO_2 nanocomposite plays a crucial role in preventing coated tinplate from corrosion. Figure 13(b) shows the hardness values of pure EP, EP−SnO_2, EP−P(Asn-co-Phe) and EP−P(Asn-co-Phe)/SnO_2 nanocomposite coated tinplate before and after immersion in 0.1 mol/L HCl. The hardness values before immersion for EP, EP−SnO_2, EP−P(Asn-co-Phe) and EP−P(Asn-co-Phe)/SnO_2 are found to be 270, 400, 500 and 650 MPa, respectively. However, the hardness values of EP−SnO_2, EP−P(Asn-co-Phe) and EP−P(Asn-co-Phe)/SnO_2 nanocomposite are found to be 201, 299 and 550 MPa, respectively, after immersion for 240 h in 0.1 mol/L HCl acid medium. The hardness value of EP−P(Asn-co-Phe)/SnO_2 nanocomposite is found to be higher even after 240 h of immersion in acidic medium in comparison with EP coating (80 MPa). Tensile strength values of pure EP, EP−SnO_2, EP−P(Asn-co-Phe), and EP−P(Asn-co-Phe)/SnO_2 nanocomposite coated tinplate before and after immersion in 0.1 mol/L HCl are shown in Fig. 13(c). Before immersion, the tensile strengths of EP, EP−SnO_2, EP−P(Asn-co-Phe), and EP−P(Asn-co-Phe)/SnO_2 are 50, 70, 90, and 110 MPa, respectively. After 240 h of immersion in 0.1 mol/L HCl, the tensile strength of pure epoxy samples drops to 20 MPa, while EP−P(Asn-co-Phe)/SnO_2 nanocomposite reaches 90 MPa. Van der Waals forces increases due to the increase in the number

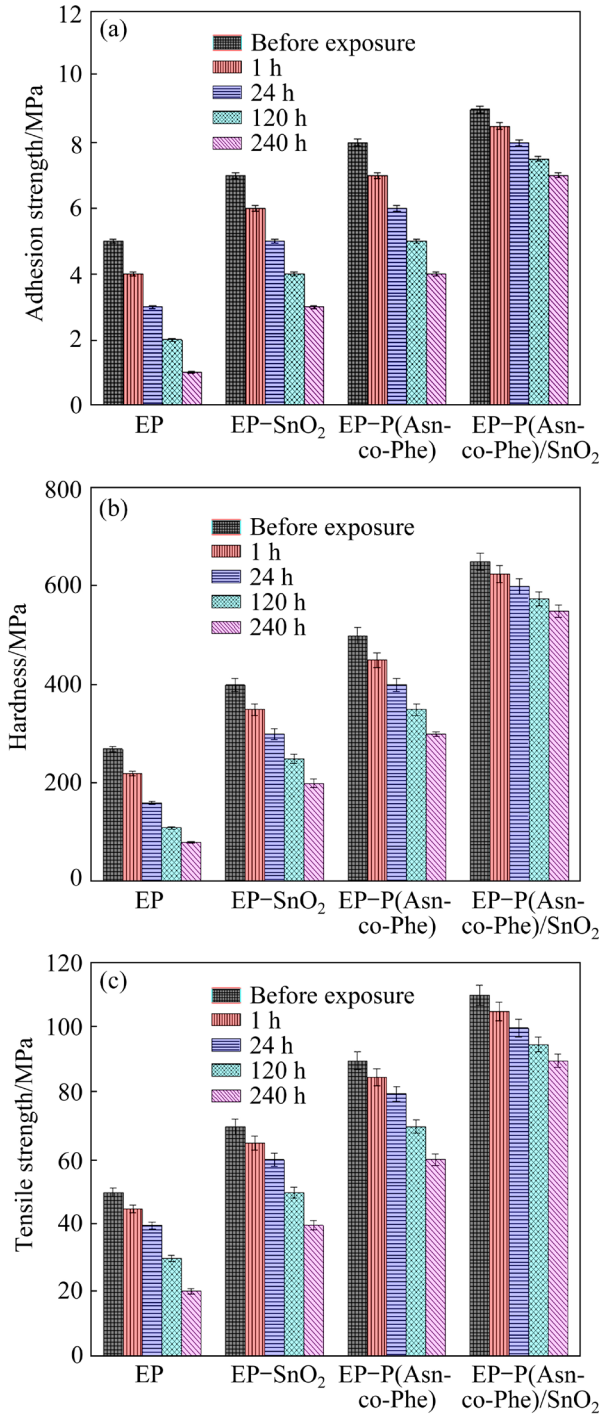

Fig. 13 Results of adhesion strength (a), hardness (b), and tensile strength (c) of pure epoxy resin (EP), EP−SnO_2, EP−P(Asn-co-Phe) and EP−P(Asn-co-Phe)/SnO_2 nanocomposite coated tinplate before and after different time of immersion in 0.1 mol/L HCl (Average values of the samples (error bars = standard deviation), calculated on 10 different samples; *p-value<0.05)

of electrons present and size of the molecule. Larger molecules have a larger "surface area" of its electron cloud, this also becoming subject to stronger Van der Walls forces. The findings show that functionalizing SnO_2 with P(Asn-co-Phe) and incorporating it (P(Asn-co-Phe)/SnO_2) into epoxy-based coatings is a potential way to build multi-functional coatings with corrosion resistance and adhesion strength. The existence of organic−inorganic functional groups in the sol−gel network is responsible for these results. Strong covalent bonds can promote adhesion and provide a barrier effect that protects the substrate from corrosion. The inclusion of SnO_2 nanoparticles into the polymer matrix enhances the flexibility and surface roughness by weakening the Vander der Waals force. As a result, the tinplate is protected from degradation by its improved adhesion strength, hardness, and tensile strength.

3.6 Oxygen and water permeability test for coated tinplate

Figure S5(a) in Supplementary Material shows the permeability of oxygen for EP, EP−SnO_2, EP−P(Asn-co-Phe) and EP−P(Asn-co-Phe)/SnO_2 nanocomposite coated tinplate before and after different time of immersion in 0.1 mol/L HCl. After 1 h of immersion, the permeation of oxygen for neat epoxy is initially less; it is achieved to be 2.5×10^{-2} mL·mm/(1.01×10^5 m^2·d·Pa)). The oxygen permeation can increase with increase of immersion time (5.0×10^{-2} mL·mm/(1.01×10^5 m^2·d·Pa) after 240 h owing to the development of large micro-pores in the coating surface. The incorporation of P(Asn-co-Phe)/SnO_2 to the epoxy polymer disrupts crystallinity and holds hydroxyl groups that could normally be associated in hydrogen bonding with oxygen and lowers the oxygen permeation. The P(Asn-co-Phe)/SnO_2 composites can enhance the oxygen barrier property of the film by developing a tortuous path. The results are found to be 2.25×10^{-2}, 1.75×10^{-2} and 0.5×10^{-2} mL·mm/(1.01×10^5 m^2·d·Pa) for EP−SnO_2, EP−P(Asn-co-Phe) and EP−P(Asn-co-Phe)/SnO_2, respectively, after 240 h of immersion. The EP−P(Asn-co-Phe)/SnO_2 nano-composite shows decreased oxygen permeability in comparison to pure EP and EP−P(Asn-co-Phe) coatings. The crystalline nature and excellent dispersion of SnO_2 nanoparticles in the polymer matrix contribute to the reduced gas permeability. The gas permeability barrier studies indicate that the EP−P(Asn-co-Phe)/SnO_2 nanocomposite coating is more susceptible and excellent gas barrier material to prevent from corrosion.

Figure S5(b) in Supplementary Material shows the permeability of water for pure EP, EP−SnO_2, EP−P(Asn-co-Phe) and EP−P(Asn-co-Phe)/SnO_2 nanocomposite coated tinplate before and after different time of immersion in 0.1 mol/L HCl. The water permeability of neat epoxy (12.2% water content) is higher than that of EP−SnO_2 (8.1% water content), EP−P(Asn-co-Phe) (5.2% water content) and EP−P(Asn-co-Phe)/SnO_2 (0.9% water content) nanocomposites after 240 h of exposure to the electrolyte. It is observed that the incorporation of P(Asn-co-Phe)/SnO_2 to epoxy resin shows decreased water absorption in the coatings. This decrease in values is most likely due to improved miscibility and dispersion, which leads to an increase in tortuosity in the matrix, which can limit the humidity or water vapour movement.

3.7 Antimicrobial activity

The agar well diffusion method was used to determine the antibacterial properties of EP−P(Asn-co-Phe)/SnO_2 nanocomposite against GNB (*E. coli*, *P. aeruginosa*), and GPB (*S. aureus*). Figure 14 displays the zones of inhibition showing the antibacterial activity of EP and EP−P(Asn-co-Phe)/SnO_2 nanocomposite. Table S1 in Supplementary Material shows a definite zone of inhibition emerging around the wells as a result of activity. The results show that the EP−P(Asn-co-Phe)/SnO_2 nanocomposite in wells increases the antibacterial activity as compared with pure EP. Although the specific mechanism of EP−P(Asn-co-Phe)/SnO_2 nanocomposite's antibacterial action is unknown, it is thought that the release of Sn cations in aqueous solution has the ability to limit the growth of bacterial species. Rather than GPB, the EP−P(Asn-co-Phe)/SnO_2 nanocomposite demonstrates stronger action against GNB. This is due to differences in the chemical structure of both types of bacteria's cell walls. The strong peptidoglycan layer present in the cell wall of GPB provides higher strength and resistance to EP−P(Asn-co-Phe)/SnO_2 nanocomposite invasion. The cell wall of GNB, on the other hand, is made up of a soft layer of peptidoglycan that allows penetrating agents to enter more easily. The increased activity of EP−P(Asn-co-Phe)/SnO_2 nanocomposite against GNB could also be attributed to the strong negative surface caused by the presence of phospholipid and lipopolysaccharide, which give a binding site for Sn cation to adhere to bacteria's surface and rip the outer membrane. Due to the presence of teichoic acid, the partly negative surface of GPB acts as a poor binding site for metal cations, resulting in minimal growth inhibition. Sn cation, super oxide radical anions, and hydroxyl radicals are formed in an aqueous suspension of EP−P(Asn-co-Phe)/SnO_2 nanocomposite. The EP−P(Asn-co-Phe)/SnO_2 nanocomposite releases Sn ions, which bind with the thiol group of a crucial bacterial enzyme, inactivating and killing microorganisms. When light strikes the EP−P(Asn-co-Phe)/SnO_2 nanocomposite surface, electrons are excited, which produces oxygen ions in interaction with absorbed oxygen, resulting in the creation of H_2O_2 when combined with H_2O molecules. As a result of entering into the bacterial cell, H_2O_2 disrupts cytoplasmic activities and proves lethal to the germs.

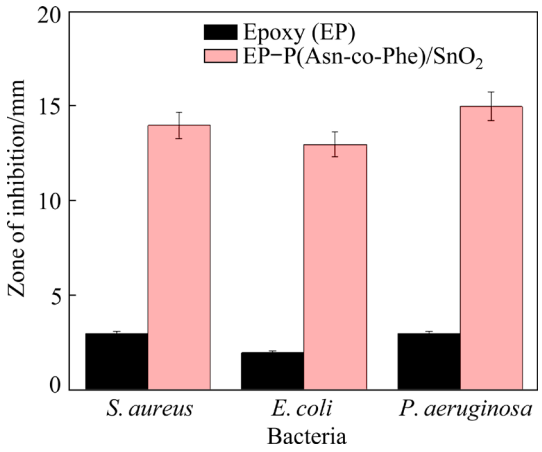

Fig. 14 Zones of inhibition showing antibacterial activity of EP and EP−P(Asn-co-Phe)/SnO_2 nanocomposite

4 Conclusions

(1) The SnO_2 nanoparticle was functionalized with poly(asparagine-co-phenyl alanine) and incorporated to epoxy resin coated tinplate. From the EIS and SECM studies, it is revealed that the EP−P(Asn-co-Phe)/SnO_2 shows better corrosion protection performance than the pure epoxy resin.

(2) The creation of a dense layer over the substrate is caused by the good dispersion of SnO_2 nanoparticles in the polymer matrix. SnO_2 in particular shields the tinplate from corrosion, preventing oxide formation and thus maintaining the coating integrity. The coating resistance is increased by adding up to 4% P(Asn-co-Phe)/SnO_2 nanocomposite to the epoxy coating.

(3) SEM scans of SnO_2 reveal spherical-shaped particles, while XRD examination confirms the sample to be crystalline with a tetragonal form.

(4) With longer immersion time in 0.1 mol/L HCl, mechanical characteristics of coated tinplate are deteriorated. Furthermore, the EP−P(Asn-co-Phe)/SnO_2 nanocomposites outperform the pure epoxy coated substrate in terms of adhesion, tensile strength, and hardness.

(5) The antibacterial activity of EP−P(Asn-co-Phe)/SnO_2 nanocomposite against GNB is found to be higher than that of GPB, which is attributed to differences in cell wall composition and surface negative charge.

(6) The EP−P(Asn-co-Phe)/SnO_2 films can be used as the potential food packaging materials in the food industry.

Supplementary Material

Supplementary Material in this paper can be found at: http://tnmsc.csu.edu.cn/download/15-p2136-2022-0238-Supplementary_Material.pdf.

References

[1] ZHANG Xian-man, CHEN Zai-yu, LUO Hong-feng, ZHOU Teng, ZHAO Yu-liang, LING Zi-cheng. Corrosion resistances of metallic materials in environments containing chloride ions: A review [J]. Transactions of Nonferrous Metals Society of China, 2022, 32: 377−410.

[2] DENG Cheng-man, ZHU Yu, SUN Sheng-kai, WEI Jun-sheng, XIA Da-hai. Analysis of failure causes of epoxy-phenolic coated tinplate after boiling sterilization [J]. Engineering Failure Analysis, 2022, 135: 106129. https://doi.org/10.1016/j.engfailanal.2022.106129.

[3] XIA Da-hai, SONG Shi-zhe, WANG Ji-hui, BI Hui-chao, JIANG Yu-xuan, HAN Zhe-wen. Corrosion behavior of tinplate in NaCl solution [J]. Transactions of Nonferrous Metals Society of China, 2012, 22: 717−724.

[4] QIU Zai-meng, ZENG Rong-chang, ZHANG Fen, SONG Liang, LI Shuo-qi. Corrosion resistance of Mg−Al LDH/Mg$(OH)_2$/silane−Ce hybrid coating on magnesium alloy AZ31 [J]. Transactions of Nonferrous Metals Society of China, 2020, 30: 2967−2979.

[5] HASHEMZADEH M, RAEISSI K, ASHRAFIZADEH F, HAKIMIZAD A, SANTAMARIA M. Incorporation mechanism of colloidal TiO_2 nanoparticles and their effect on properties of coatings grown on 7075 Al alloy from silicate-based solution using plasma electrolytic oxidation [J]. Transactions of Nonferrous Metals Society of China, 2021, 31: 3659−3676.

[6] HUANG Xian-qiu, LANG Feng-jun, MA Ying, CHEN Yu, ZHANG Zhao, ZHANG Jian-qing. Effects of reflowing temperature and time on alloy layer of tinplate and its electrochemical behavior in 3.5% NaCl solution [J]. Transactions of Nonferrous Metals Society of China, 2014, 24: 1978−1988.

[7] ZHANG Yi-tong, LIU Xiao-yun, ZHAN Guo-zhu, ZHUANG Qi-xin, ZHANG Ru-hong, QIAN Jun. Study on the synergistic anticorrosion property of a fully bio-based polybenzoxazine copolymer resin [J]. European Polymer Journal, 2019, 119: 477−486.

[8] LUZI F, TORRE L, PUGLIA D. Antioxidant packaging films based on ethylene vinyl alcohol copolymer (EVOH) and caffeic acid [J]. Molecules, 2020, 25(17): 3953. https://doi.org/10.3390/molecules25173953.

[9] ZUMELZU E, SILVA E, RULL F, MUNOZ O, UGARTE R. Effect of lactic acid on polyethylene terephthalate (PET) and polypropylene (PP) coatings of food containers [J]. Journal of Polymers and the Environment, 2018, 26: 2476−2488.

[10] VILLEGAS C, ARRIETA M P, ROJAS A, TORRES A, FABA S, TOLEDO M J, GUTIERREZ M A, ZAVALLA E, ROMERO J, GALOTTO M J, VALENZUELA X. PLA/organoclay bionanocomposites impregnated with thymol and cinnamaldehyde by supercritical impregnation for active and sustainable food packaging [J]. Composites Part B: Engineering, 2019, 176: 107336. https://doi.org/10.1016/j.compositesb.2019.107336.

[11] MALLAKPOUR S, MADANI M. Use of L-tyrosine amino acid as biomodifier of Cloisite Na^+ for preparation of novel poly(vinyl alcohol)/organoclay bionanocomposites film [J]. Journal of Materials Science, 2011, 46: 4071−4078.

[12] YAN Ting-liang, WANG Xiang, FAN Jin-long, NIE Qi-dong. Microstructure and properties of biodegradable co-continuous (HA+β-TCP)/Zn−3Sn composite fabricated by vacuum casting-infiltration technique [J]. Transactions of Nonferrous Metals Society of China, 2021, 31: 3075−3086.

[13] LI Qing-hua, ZHOU Qin-hua, DENG Dan, YU Qiao-zhen, GU Li, GONG Ke-da, XU Ke-hang. Enhanced thermal and electrical properties of poly (D,L-lactide)/multi-walled carbon nanotubes composites by in-situ polymerization [J]. Transactions of Nonferrous Metals Society of China, 2013, 23: 1421−1427.

[14] TSAGKARIS A S, TZEGKAS S G, DANEZIS G P. Nanomaterials in food packaging: State of the art and analysis [J]. Journal of Food Science and Technology, 2018, 55: 2862−2870.

[15] ABDULLAH Z W, DONG Y. Recent advances and perspectives on starch nanocomposites for packaging applications [J]. Journal of Materials Science, 2018, 53: 5319−15339.

[16] GARCIA C V, SHIN G H, KIM J T. Metal oxide-based nanocomposites in food packaging: Applications, migration, and regulations [J]. Trends in Food Science & Technology, 2018, 82: 21−31.

[17] REHMAN S, ASIRI S M, KHAN F A, JERMY B R, KHAN H, AKHTAR S, AL JINDAN R, KHALID KHAN M, QURASHI A. Biocompatible tin oxide nanoparticles:

Synthesis, antibacterial, anticandidal and cytotoxic activities [J]. ChemistrySelect, 2019, 4: 4013−4017.

[18] SHARMA S, SINGH A A, MAJUMDAR A, BUTOLA B S. Tailoring the mechanical and thermal properties of polylactic acid-based bionanocomposite films using halloysite nanotubes and polyethylene glycol by solvent casting process [J]. Journal of Materials Science, 2019, 54: 8971−8983.

[19] VENKATESAN R, RAJESWARI N. Poly(butylene adipate-co-terephthalate) bio nanocomposites: Effect of SnO_2 NPs on mechanical, thermal, morphological, and antimicrobial activity [J]. Advanced Composites and Hybrid Materials, 2018, 1: 731−740.

[20] SILVA A L C, UGUCIONI J C, CORREA S, ARDISSON J D, MACEDO W A A, SILVA J P, COTTA A A C, BRITO A D B. Synthesis and characterization of nanocomposites consisting of polyaniline, chitosan and tin dioxide [J]. Materials Chemistry and Physics, 2018, 216: 402−412.

[21] KHASIM S, PASHA A. Enhanced corrosion protection of A-36 steel using epoxy-reinforced CSA-doped polyaniline−SnO_2 nanocomposite smart coatings [J]. Journal of Bio- and Tribo-Corrosion, 2021, 7: 26. https://doi.org/10.1007/s40735-020-00455-7.

[22] ZOR S, ILMIEVA N. Corrosion behavior of PANI/epoxy/nano SnO_2 polymeric nanocomposite coated stainless steel in 3.5 wt.% NaCl [J]. Polymer Composites, 2018, 39: E2415−E2425.

[23] XAVIER J R. Electrochemical, mechanical and adhesive properties of surface modified NiO−epoxy nanocomposite coatings on mild steel [J]. Materials Science and Engineering B, 2020, 260: 114639. https://doi.org/10.1016/j.mseb.2020.114639.

[24] ZHOU Xing-nan, HUANG Hao-wei, ZHU Rui, SHENG Xin-xin, XIE De-long, MEI Yi. Facile modification of graphene oxide with Lysine for improving anticorrosion performances of water-borne epoxy coating [J]. Progress in Organic Coatings, 2019, 136: 105200. https://doi.org/10.1016/j.porgcoat.2019.06.046.

[25] DÍEZ-PASCUAL A M. Poly(3-hydroxybutyrate-co-3- hydroxyhexanoate) with zinc oxide nanoparticles for food packaging [J]. Journal of Food Process Engineering, 2021, e13814. https://doi.org/10.1111/jfpe.13814.

[26] JESHURAN R B, XAVIER J R. Mechanical and corrosion protection properties of polymer–clay nanocomposite coatings for mild steel in marine environment [J]. Emergent Materials, 2020, 3: 75−85. https://doi.org/10.1007/s42247-020-00073-6.

[27] AZIZ M, ABBAS S S, BAHAROM W R W. Size-controlled synthesis of SnO_2 nanoparticles by sol−gel method [J]. Materials Letters, 2013, 91: 31−34.

[28] XAVIER J R, JESHURAN R B, VINODHINI S P. Novel multifunctional nanocomposites for superior barrier, hydrophobic and mechanical properties of Mg alloy in marine environment [J]. Surface & Coatings Technology, 2021, 421: 127475. https://doi.org/10.1016/j.surfcoat.2021.127475.

[29] KONDAWAR S B, AGARWAL S P, NIMKAR S H, SHARMA H J, PATIL P T. Conductive polyaniline-tin oxide nanocomposites for ammonia sensor [J]. Advanced Materials Letters, 2012, 3(5): 393−398.

[30] PATIL D, PATIL P, SEO Y K, HWANG Y K. Poly-(o-anisidine)–tin oxide nanocomposite: Synthesis, characterization and application to humidity sensing [J]. Sensors and Actuators B, 2010, 148: 41−48.

[31] FU L, ZHENG Y, REN Q, WANG A, DENG B. Green biosynthesis of SnO_2 nanoparticles by *Plectranthus Amboinicus* leaf extract their photocatalytic activity towards Rhodamine B Degradation [J]. Journal of Ovonic Research, 2015, 11(1): 21−26.

[32] PATIL S S, HARPALE K V, KOIRY S P, PATIL K R, ASWAL D K, MORE M A. Multifunctional polyaniline–tin oxide (PANI−SnO_2) nanocomposite: Synthesis, electrochemical, and field emission investigations [J]. Journal of Applied Polymer Science, 2015, 132: 41401. doi: 10.1002/app.41401.

[33] XAVIER J R. Electrochemical and dynamic mechanical properties of polyurethane nanocomposite reinforced with functionalized TiO_2−ZrO_2 nanoparticles in automobile industry [J]. Appl Nanosci, 2022, 12: 1763−1778.

[34] VINODHINI S P, XAVIER J R. Effect of graphene oxide wrapped functional silicon carbide on structural, surface protection, water repellent, and mechanical properties of epoxy matrix for automotive structural components [J]. Colloids and Surfaces A: Physicochemical and Engineering Aspects, 2022, 639: 128300. https://doi.org/10.1016/j.colsurfa.2022.128300.

[35] EL-SHERIF R M, BADAWY W A. Mechanism of corrosion and corrosion inhibition of tin in aqueous solutions containing tartaric acid [J]. International Journal of Electrochemical Science, 2011, 6: 6469−6482.

[36] EL IBRAHIMI B, JMIAI A, BAZZI L, ISSAMI S E. Amino acids and their derivatives as corrosion inhibitors for metals and alloys [J]. Arabian Journal of Chemistry, 2020, 13(1): 740−771.

[37] XAVIER J R. Novel multilayer structural epoxy nanocomposite coating for enhanced adhesion and protection properties of steel [J]. Polymer-Plastics Technology and Materials, 2022, DOI: 10.1080/25740881.2022.2071160.

[38] XAVIER J R, VINODHINI S P, SRINIVASAN N. Effects of incorporating silanized nanoclay on the barrier, hydrophobic and mechanical properties of epoxy resin in chloride environment [J]. Ind Eng Chem Res, 2022, 61: 6973−6986.

耐化学腐蚀和疏水性的食品包装用含 SnO_2 生物纳米复合材料

Joseph Raj XAVIER[1], C. DHANALAKSHMI[2], Shanmuga Sundari CHANDRARAJ[2], S. P. VINODHINI[1]

1. Department of Chemistry, Saveetha School of Engineering,
Saveetha Institute of Medical and Technical Sciences, Chennai-602 105, Tamil Nadu, India;
2. Department of Chemistry, Vel Tech Rangarajan Dr. Sagunthala R&D Institute of Science and Technology,
Chennai-600 062, Tamil Nadu, India

摘　要：研究了聚(天冬酰胺-共苯丙氨酸)(P(Asn-co-Phe)/SnO_2)对环氧树脂(EP)涂层防护性能的影响。电化学阻抗谱分析表明，与纯环氧树脂涂层相比，马口铁表面 EP−P(Asn-co-Phe)/SnO_2 纳米复合材料涂层具有更好的防护作用。EP−P(Asn-co-Phe)/SnO_2 纳米复合材料涂层的电阻(R_{coat})为 3854.70 kΩ·cm^2，比环氧树脂涂层的大 38 倍。扫描电化学显微镜分析表明，EP−P(Asn-co-Phe)/SnO_2 的电流分布更小。通过 XRD 和 SEM/EDX 对降解产物进行分析，证实了功能化 SnO_2 颗粒对环氧树脂涂层防护能力的影响。EP−P(Asn-co-Phe)/SnO_2 纳米复合材料涂层的水接触角为 133°，证实了其疏水性。此外，与纯环氧树脂涂层相比，EP−P(Asn-co-Phe)/SnO_2 纳米材料复合涂层具有更高的力学性能和抗菌活性。综上，由于在环氧树脂基体中添加了 P(Asn-co-Phe)/SnO_2 纳米颗粒，EP−P(Asn-co-Phe)/SnO_2 纳米复合材料提供了出色的屏障和力学性能，从而阻碍了材料的降解，有助于延长涂层钢的寿命。

关键词：马口铁；环氧树脂；SnO_2；纳米材料复合涂层；共聚物；热稳定性；硬度

(Edited by Bing YANG)